J. Synchrotron Rad. (1995). **2**, 264–271

Resonant Photoemission from Complex Cuprates and Nickelates

W. R. Flavell,[a]* J. Hollingworth,[a] J. F. Howlett,[a] A. G. Thomas,[a] Md. M. Sarker,[a] S. Squire,[a] Z. Hashim,[a] M. Mian,[a] P. L. Wincott,[b] D. Teehan,[c] S. Downes[c] and F. E. Hancock[d]

[a]*Department of Chemistry, UMIST, PO Box 88, Manchester M60 1QD, UK,* [b]*Department of Chemistry/IRCSS, University of Manchester, Manchester M13 9PL, UK,* [c]*CLRC Daresbury Laboratory, Daresbury, Warrington, Cheshire WA4 4AD, UK, and* [d]*ICI Katalco, RT&E, PO Box 1, Billingham, Cleveland TS23 1LB, UK*

(*Received 25 April 1995; accepted 19 June 1995*)

Synchrotron-excited resonant-photoemission measurements at rare-earth $4d \rightarrow 4f$ and transition-metal $3p \rightarrow 3d$ thresholds have been carried out using a variety of complex cuprates and nickelates on stations 6.1 (grazing-incidence monochromator) and 6.2 (toroidal-grating monochromator) at the SRS CLRC Daresbury Laboratory. The systems studied are $Nd_2Ni_{1-x}Cu_xO_4$, $La_{2-x}Sr_xNi_{1-y}Fe_yO_{4+\delta}$ and $Bi_2Sr_2Ca_{1-x}Y_xCu_2O_{8+\delta}$. A combination of EDC and constant-initial-state data is used to examine the $4f$ and $3d$ contributions to the valence-band density of states and their binding-energy positions relative to the Fermi energy. This allows the study of the valence states of the transition-metal ions and their modulation on doping. For $La_{2-x}Sr_xNi_{1-y}Fe_yO_{4+\delta}$, this approach is used to infer a valence state of ≥ 3.0 for Fe. In the case of $Bi_2Sr_2Ca_{1-x}Y_xCu_2O_{8+\delta}$, the effect of Cu valence modulation on the $3p$ resonance is observed as x is varied. This is discussed in the light of controversy surrounding shifts in core-level photoemission with doping for this system.

Keywords: resonant photoemission; complex cuprate; complex nickelate; 3*p* threshold; 4*d* threshold.

1. Introduction

The electronic structure of complex cuprates and nickelates is of considerable interest, as the properties of these oxides may be tailored to specific applications by subtle changes in chemical doping. This can allow the electronic conduction of the material to be tuned from insulating to metallic and even superconducting. In addition, it may be possible to stabilize certain ions (particularly transition-metal ions) in unusual valence states, leading to potential applications in oxidation catalysis. Modulation of the formal valency of the transition-metal ion in these systems may be achieved by doping at a counter-cation site. Often the counter cations may be rare-earth elements, and in this case, the valence modulation achieved is dependent on the relative positions of the $4f$ and $3d$ contributions within the valence-band density of states (DOS) relative to the Fermi energy (as this is equivalent to the chemical potential of the system).

Synchrotron-excited resonant photoemission is exceptionally powerful in revealing the atomic character of these states. Here we apply the technique to three families of complex mixed transition-metal/rare-earth oxides, $Nd_2Ni_{1-x}Cu_xO_4$, $La_{2-x}Sr_xNi_{1-y}Fe_yO_{4+\delta}$ and $Bi_2Sr_2Ca_{1-x}Y_xCu_2O_{8+\delta}$.

$Bi_2Sr_2Ca_{1-x}Y_xCu_2O_{8+\delta}$ ($x = 0$, BCSCO 2212) is a cuprate superconductor with a superconducting transition temperature, T_c, of 85 K. The presence of superconductivity in this material seems associated with the maintenance of an unusually high formal Cu valency in this material of > 2.0. On replacing divalent Ca by trivalent Y, the formal copper valency is reduced towards 2.0, and the material undergoes a metal-to-non-metal transition when about half the Ca is replaced (Manthiram & Goodenough, 1988; Tamegai *et al.*, 1989; Groen, de Leeuw & Feiner, 1990). This transition has been studied in a number of photoemission measurements, which show the disappearance of the DOS at the Fermi level as the transition is approached, with a corresponding shift in valence-band and core-level peaks (*e.g.* van Veenendaal, Sawatzky & Groen, 1994; van Veenendaal, Schlatmann, Sawatzky & Groen, 1993; Itti *et al.*, 1991; Golden, Golden, Egdell & Flavell, 1991). The valence modulation caused by the addition of Y is accompanied by structural modifications, primarily contraction along the c axis of the structure, and expansion in the ab plane, which contains the Cu–O_2 planes, with corresponding changes in Cu–O hybridization (Manthiram & Goodenough, 1988; Tamegai *et al.*, 1989; Groen *et al.*, 1990). Here we observe the effect of the valence modulation on the Cu $3p \rightarrow 3d$ resonance in synchrotron-excited photoemission.

* Author to whom correspondence should be addressed.

$La_{2-x}Sr_xNiO_{4+\delta}$ is the nickel analogue of the cuprate superconductor $La_{2-x}Sr_xCuO_{4+\delta}$. In common with this material, the formal transition-metal valency can be raised above 2.0 by replacement of trivalent La by divalent Sr, and the material also undergoes a non-metal-to-metal transition as x increases. In contrast with the cuprate, which becomes metallic for small values of x, the metallic phase in the nickelate is not achieved until x reaches at least 0.8 (Benloucif, Nguyen, Greneche & Raveau, 1991), at which point the majority of the Ni is in the Ni^{III} oxidation state. There have been very few studies of iron doping in this material, but Mössbauer studies suggest that Fe can be maintained in the Fe^{IV} state in this material (Benloucif *et al.*, 1991). Thus, in common with the cuprates, in this lattice, the transition-metal ions appear to be stabilized in unusually high oxidation states. One measurement has probed the Ni contribution to the valence-band DOS function in the $y = 0$ material $La_{2-x}Sr_xNiO_4$ (Eisaki *et al.*, 1992), using Ni $3p \rightarrow 3d$ resonant photoemission. Here, we use this resonance to study the Ni DOS in Fe co-doped materials, and also use the corresponding Fe resonance to provide complementary information about the Fe valence-band DOS.

Nd_2NiO_4 is the Ni analogue of the cuprate Nd_2CuO_4. The latter material becomes superconducting on doping with Ce, to give $Nd_{2-x}Ce_xCuO_4$, and is one of very few 'electron-doped' superconducting materials known (Tokura, Takagi & Uchida, 1989). The doping mechanism is rationalized as replacement of trivalent Nd by four-valent Ce, giving rise to a reduction in the Cu formal valence state to < 2.0. The implication of this is that Cu^{I} may be stabilized in this structure in the presence of Ce^{IV}, certainly not a result which would be expected in solution. Here we explore the potential of the mixed system $Nd_2Ni_{1-x}Cu_xO_4$ for the stabilization of the transition-metal ions Ni and Cu in unusually low oxidation states by introduction of another rare-earth element for Nd. In this initial study, we concentrate on the $4f$ contribution to the valence-band DOS.

2. Experimental

Ceramic samples of the complex nickelates and cuprates were prepared by solid-state or solution routes. $Nd_2Ni_{1-x}Cu_xO_4$ was prepared from stoichiometric amounts of NiO, CuO and Nd_2O_3, which were ground together and annealed in air at 1423 K for 100 h, and then in oxygen at 1173 K for 20 h. $La_{2-x}Sr_xNi_{1-y}Fe_yO_{4+\delta}$ was produced by a co-precipitation route. Stoichiometric amounts of $LaCl_3.7H_2O$, $Sr(NO_3)_2$, $NiCl_2.6H_2O$ and $Fe(NO_3)_3.9H_2O$ were dissolved in distilled water. The solution pH was adjusted to 9 by addition of saturated Na_2CO_3 solution, and the resulting precipitate was filtered, washed and dried overnight at 393 K. The glassy material was then ground and annealed at 1170 K for 10 h, before being reground and annealed at 1473 K for 48 h. After a further regrinding, the material was annealed under oxygen for 20 h at 1443 K. $Bi_2Sr_2Ca_{1-x}Y_xCu_2O_{8+\delta}$ was prepared *via* a solid-state route from Bi_2O_3, $SrCO_3$, Y_2O_3, $CaCO_3$ and CuO. These were mixed in stoichiometric proportions, and initially annealed at 1053 K overnight to drive off carbonate. The mixture was then reground and successively annealed in air at 1073, 1093, 1113 and 1133 K for 16 h each, with regrinding at each stage. Finally, the samples were fired for 7–9 days at 1143 K in air, with intermittent regrindings (Weller, 1992).

In all cases the samples were characterized by X-ray diffraction (XRD), energy dispersive X-ray analysis (EDAX), and in some cases atomic absorption spectrophotometry (AA). X-ray diffraction was carried out using a Scintag XDS2000 automated powder diffractometer and monochromated Cu $K\alpha$ radiation. EDAX investigations were carried out in order to check the bulk composition of the samples synthesized, using a Philips SEM 505 microscope with a 9100/60 system attachment for EDAX. In some cases AA measurements were additionally carried out in order to quantify low doping levels. These used a Thermo-Jarrell-Ash Video 22E atomic absorption spectrophotometer. The $Bi_2Sr_2Ca_{1-x}Y_xCu_2O_{8+\delta}$ samples were additionally characterized by vibrating sample magnetometry (VSM), using an Oxford Instruments machine with a 50 Oe (3979 A m^{-1}) field.

Resonant-photoemission measurements were carried out at the Synchrotron Radiation Source, CLRC Daresbury Laboratory. These measurements used the grazing-incidence monochromator ($30 \leq h\nu \leq 220$ eV) on station 6.1 and the toroidal-grating monochromator ($15 \leq h\nu \leq 90$ eV) on station 6.2, both with a Phi double-pass CMA. The position of the Fermi edge was determined by reference to the Mo sample holder. For introduction into UHV, the powder samples were pressed into pellets, and these were reannealed under conditions identical to those used for the final stage of the relevant synthesis, giving mechanical strength to the pellets. Sections of these were mounted onto an Mo sample plate using silver-loaded UHV-compatible epoxy resin. The surfaces of the materials to be studied were cleaned for UHV measurements by scraping using a diamond file in vacua of 5×10^{-11}–10^{-10} mbar. Sample cleanliness was monitored using the valence-band photoemission in the range 5–15 eV binding energy. The characteristic adsorption features which arise in the valence-band photoemission due to surface contamination were established in a separate series of experiments involving the adsorption of small probe molecules normally present in the residual vacuum, such as CO and H_2O (Howlett *et al.*, 1995).

3. Results and discussion

3.1. *Bulk characterization*

Powder X-ray diffraction measurements from $Nd_2Ni_{1-x}Cu_xO_4$ indicated that the system maintains the monoclinic structure of Nd_2NiO_4 in the range $x = 0$–0.25. For $x = 0.5$, peaks due to both the Nd_2NiO_4 structure and tetragonal Nd_2CuO_4 are apparent, the peaks due to the nickelate decreasing in intensity in the range

x = 0.5–1.0 (all cuprate). In our photoemission work, we have concentrated on the single-phase regime, and data presented below refer to a single-phase compound with x = 0.25.

XRD from $La_{2-x}Sr_xNi_{1-y}Fe_yO_{4+\delta}$ (x = 0–1, y = 0–0.2) showed the samples to be highly crystalline and essentially single phase, although for some compositions a small number of additional peaks were visible just above the background noise level. This suggests the presence of a small amount (≤2%) of an unidentified second phase. EDAX and AA results were consistent with the bulk nominal compositions.

XRD from $Bi_2Sr_2Ca_{1-x}Y_xCu_2O_{8+\delta}$ again showed the samples to be highly crystalline. This 2212 phase is difficult to synthesize completely free of other BCSCO phases, and most XRD patterns showed the presence of a small amount (~2%) of the 2201 phase ($Bi_2Sr_2CuO_{6+\delta}$). In the case of one sample, having x = 0.4, the proportion of 2201 phase was large, up to *ca* 30%, and the Y content of this sample (as determined by EDAX) was anomalous. This sample was therefore omitted from our photoemission measurements. VSM showed the samples to be superconducting (with decreasing T_c) for Y content up to x = 0.45–0.50.

3.2. *Photoemission measurements*

3.2.1. *$Nd_2Ni_{1-x}Cu_xO_4$.* Fig. 1 shows spectra of $Nd_2Ni_{1-x}Cu_xO_4$ (x = 0.25) accumulated in EDC mode using station 6.1. These show the valence-band region (in the range 1.5–10 eV binding energy) and the low-lying Nd 5*p* levels (in the range 18–23 eV binding energy). Band-structure calculations for the related cuprate would lead us to suppose that the broad valence band contains contributions from transition-metal 3*d*, Nd 4*f* and O 2*p* states (*e.g.* Massidda, Hamada, Yu & Freeman, 1989). The contribution to this DOS from the 4*f* states can be obtained from the difference between spectra taken at and off the rare-earth $4d \rightarrow 4f$ core absorption peaks. This utilizes the interference between direct 4*f*-electron photoemission and the $4d \rightarrow 4f$ transition followed by super Coster–Kronig Auger decay:

$$4d^{10}4f^n + h\nu \rightarrow \{4d^9 4f^{n+1}\}^* \rightarrow 4d^{10}4f^{n-1} + e^-.$$

The spectra are taken at the Nd $4d \rightarrow 4f$ resonance ($h\nu$ = 128 eV) and off-resonance ($h\nu$ = 122 eV). Both spectra are normalized to the beam monitor reading. The difference spectrum (128 – 122 eV) is also shown. This shows strong Nd character across the core peaks (as expected), but also a very extensive 4*f* contribution to the valence-band density of states, which has peaks at ~4 and ~7 eV binding energy. This result is in very good agreement with the resonant photoemission of $Nd_{2-x}Ce_xCuO_4$ (*e.g.* Namatame *et al.*, 1990), and is characteristic of the $4f^3$ ground state of Nd^{III}. The lower binding-energy peak arises from the unscreened $4f^2$ final state, whilst the higher binding-energy feature arises from a final state in which the 4*f* hole is screened by electron transfer from the ligand (in this case from O 2*p*), giving a configuration $4f^3\underline{L}^1$ (using the conventional notation, where the bar denotes a hole). It can be seen that the Nd 4*f* contribution to the valence-band density of states is around 9 eV wide, and essentially covers the entire valence band, with the exception of the low-binding-energy valence-band edge. This result is echoed in the constant-initial-state (CIS) spectra of Fig. 2, where the photon energy is scanned through the resonance. The initial-state binding energies chosen are 1.4 eV (low-binding-energy valence-band edge), 5.1 eV (valence-band intensity maximum), 10.1 eV (high-binding-energy side of the valence band) and 19.4, 23.8 eV (Nd 5*p* core levels). The shape of the resonance is complex, essentially due to the open-shell configuration of the 4*f* levels in the photoexcited state $\{4d^9 4f^4\}^*$, leading to exchange and correlation interaction of the 4*d* hole with the 4*f* states. The same complex characteristic shape for the $4d \rightarrow 4f$ resonance is revealed at all binding-energy positions selected except the valence-band edge (E_B = 1.41 eV). This result suggests that the states closest to the valence-band edge have Ni/Cu/O rather than Nd/O character. In turn, this implies that doping a counter-cation of different valency for Nd would lead to modulation of the transition-metal-ion valency, rather than

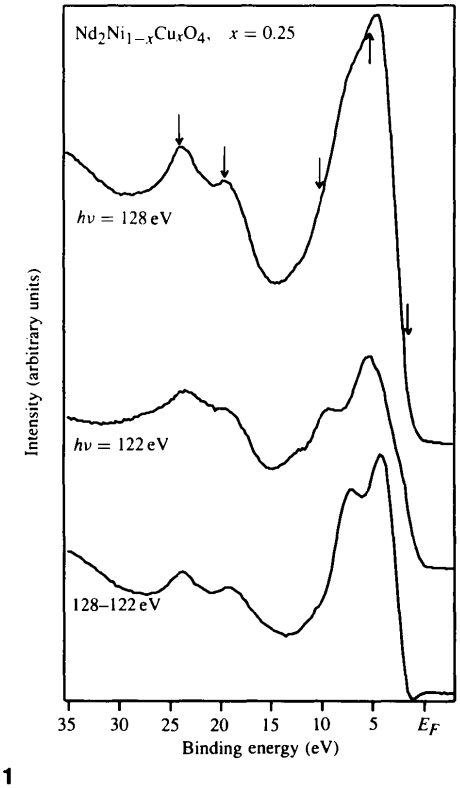

Figure 1
EDC's showing the valence-band and low-lying core levels of a scraped ceramic sample of $Nd_2Ni_{0.75}Cu_{0.25}O_4$, at the Nd $4d \rightarrow 4f$ resonance ($h\nu$ = 128 eV), off-resonance ($h\nu$ = 122 eV), and the difference spectrum, showing the characteristic valence-band signal of a $4f^3$ ground state. Note the absence of a 4*f* contribution to the valence-band edge. The spectra are normalized to the beam monitor reading. (The binding-energy positions marked by arrows refer to the initial-state positions used for the CIS measurements shown in Fig. 2.)

that of the rare earth, as in $Nd_{2-x}Ce_xCuO_4$, where Cu^I may be stabilized in the presence of Ce^{IV}.

3.2.2. *$La_{2-x}Sr_xNi_{1-y}Fe_yO_{4+\delta}$.* Resonant photoemission may also be used to probe the transition-metal valency contribution to the valence-band DOS, as shown in Figs. 3 and 4, which show EDC and CIS mode data for $La_{2-x}Sr_xNi_{1-y}Fe_yO_{4+\delta}$ recorded using station 6.2. Fig. 3 shows valence-band spectra for a sample of $La_2NiO_{4+\delta}$ recorded on-resonance ($h\nu$ = 67 eV) and off-resonance ($h\nu$ = 63 eV) at the Ni $3p \rightarrow 3d$ threshold. The feature at 9 eV binding energy is in part contaminant-related; our adsorption measurements indicate that this feature grows in intensity with CO dosing, leading to the formation of a surface carbonate-like feature (Howlett *et al.*, 1995). However, this region of the spectrum also includes a contribution from a valence-band satellite feature, as observed in NiO (Thuler, Benbow & Hurych, 1983). The difference spectrum (67–63 eV) is similar to that of Eisaki *et al.* (1992) for this material, showing a shift in overall intensity to the satellite region at resonance. Here it is evident that the observed resonance is considerably weaker than for the $d \rightarrow f$ transition, but it is nevertheless seen clearly in the CIS data of Fig. 4. Data are recorded at the valence-band edge (1.2 eV binding energy), valence-band intensity maximum (4.3 eV binding energy) and satellite feature (9.2 eV binding energy). The CIS spectra show a small anti-resonance at the valence-band edge, and a resonance at the satellite feature. This resonance behaviour is also observed for Sr- and Fe-doped samples, and is in good agreement with the data of Eisaki *et al.* (1992) for samples with $y = 0$.

$3p \rightarrow 3d$ resonant effects are seen for a wide range of transition-metal oxides, and are interpreted in a similar way to the $d \rightarrow f$ resonance described above. The processes occurring are described for a general $3d^n$ initial-state configuration below. In this case, the direct photoemission process may be written:

$$3p^6 3d^n + h\nu \rightarrow 3p^6 3d^{n-1} + e^-.$$

At photon energies larger than the $3p \rightarrow 3d$ absorption threshold, the direct process is supplemented by initial $3p \rightarrow 3d$ excitation, followed by super Coster–Kronig Auger decay:

$$3p^6 3d^n + h\nu \rightarrow \{3p^5 3d^{n+1}\}^* \rightarrow 3p^6 3d^{n-1} + e^-.$$

Resonant effects are attributed to interference between direct and indirect channels. Using this model, threshold

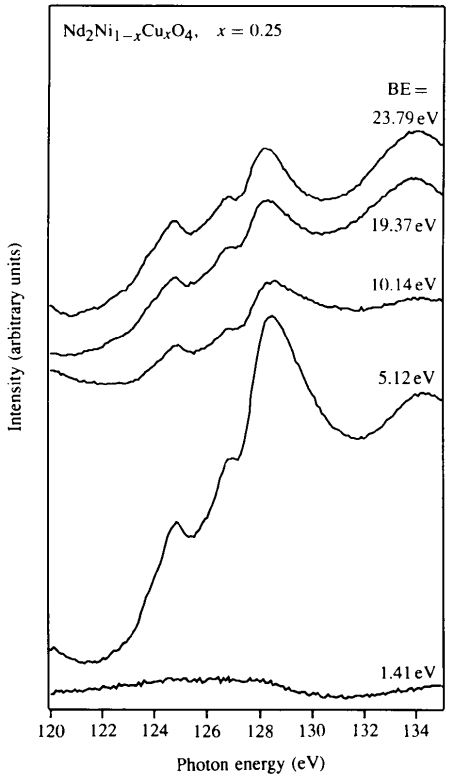

Figure 2
CIS spectra from scraped ceramic $Nd_2Ni_{0.75}Cu_{0.25}O_4$ at the valence-band edge (E_B = 1.41 eV), valence-band intensity maximum (5.12 eV), the high-binding-energy part of the valence band (10.14 eV), and the Nd 5*p* core-level peaks (19.37 and 23.79 eV), showing the characteristic shape of the Nd $4d \rightarrow 4f$ resonance at all parts of the spectrum except the valence-band edge. (The chosen initial-state binding energies are marked by arrows in Fig. 1.) Spectra are normalized to the beam monitor reading. The tungsten absorption coefficient of the beam monitor is featureless in this photon energy range.

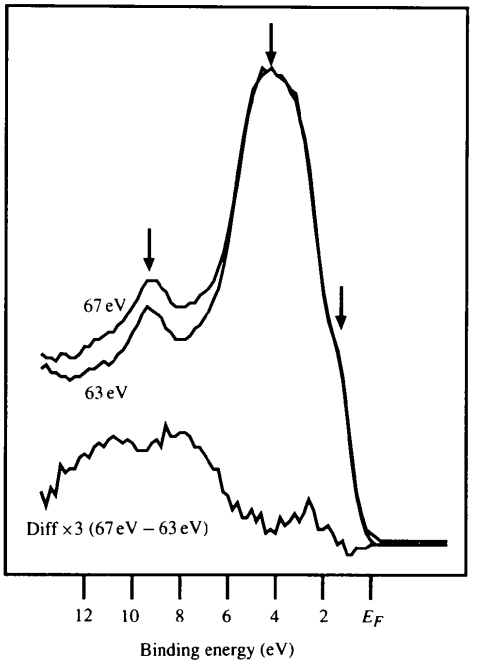

Figure 3
EDC's showing the valence-band and satellite region of a scraped ceramic sample of $La_2NiO_{4+\delta}$, at the Ni 3p $\rightarrow$ 3d resonance ($h\nu$ = 67 eV), off-resonance ($h\nu$ = 63 eV), and the difference spectrum, showing the shift in intensity towards the satellite region at resonance. Spectra are normalized to the beam monitor reading. (The binding-energy positions marked by arrows refer to the initial-state positions used for the CIS measurements shown in Fig. 4.)

resonances have been interpreted as implying strong d character in the valence-band density of states, as in an unscreened pure $3d^{n-1}$ configuration, whilst anti-resonance (where the dip in the Fano resonance shape is larger than the succeeding maximum) is interpreted as indicating a screened final state of the type $3d^n\underline{L}^1$. There is thus a significant difference between the $d \rightarrow f$ and $p \rightarrow d$ resonant processes in this respect, as the ligand-hole final state gives rise to a resonance in the former case, as we saw in Fig. 1. The observation of an anti-resonance at the $p \rightarrow d$ threshold for ligand-hole final states in the late transition-metal oxides is confirmed by cluster calculations such as those for CuO (Ghijsen, Tjeng, Eskes, Sawatzky & Johnson, 1990). The resonant behaviours observed in Fig. 4 thus confirm that the states to the low-binding-energy side of the main valence band arise mainly from Ni $d^8\underline{L}$ final states, with the satellite feature at around 9.5 eV binding energy representing the unscreened Ni d^7 configuration. The valence-band intensity maximum at *ca* 4 eV binding energy shows no resonant effect, and we attribute it to O $2p$ states, which are essentially non-bonding for samples which contain no Fe.

Fig. 5 shows corresponding CIS data taken at the Fe $3p \rightarrow 3d$ resonance for an Fe-doped sample, $La_{1.1}Sr_{0.9}Fe_{0.2}Ni_{0.8}O_{4+\delta}$. These data are typical of those taken for all Fe-doped samples, and show some Fe contribution to the DOS for all parts of the valence-band and satellite regions. In this respect the data are in good agreement with CIS spectra of simple iron oxides such as Fe_xO ($x \simeq 0.95$), Fe_3O_4 and Fe_2O_3 (Fujimori, Kimizuka, Taniguchi & Suga, 1987; Fujimori, Saeki, Kimizuka, Taniguchi & Suga, 1986; Lad & Henrich, 1989). The position of the resonance is of some interest as a guide to the Fe valency in these systems. Whereas the Ni resonance does not appear to shift significantly with change in oxidation state (Thuler *et al.*, 1983), the corresponding shifts in position of the Fe resonance appear to be quite significant (Lad & Henrich, 1989). Lad & Henrich (1989) note that the onset of the resonance depends on the oxidation state of the Fe cation, and correlates with the Fe $3p$ binding energies determined by XPS. These authors show CIS data with a resonance maximum at ~56.3 eV for Fe^0, ~57.8 eV for Fe^{II} and ~58.2 eV for Fe^{III}. In our case, the low amount of Fe dopant incorporated into the samples means that the resonances are rather weak. However, it appears that the resonance maximum is located in the range 58.2–58.6 eV. No resonant data for Fe^{IV} is available for comparison, but we suggest that the resonance position measured is indicative of a high valence state of ≥ 3.0 for Fe. The data are thus consistent with the work of Benloucif *et al.* (1991) who conclude that these materials contain predominantly Fe^{III}, but also Fe^{IV} valencies.

The resonances shown in Fig. 5 appear to be slightly stronger in the satellite region (binding energy 12.2 eV)

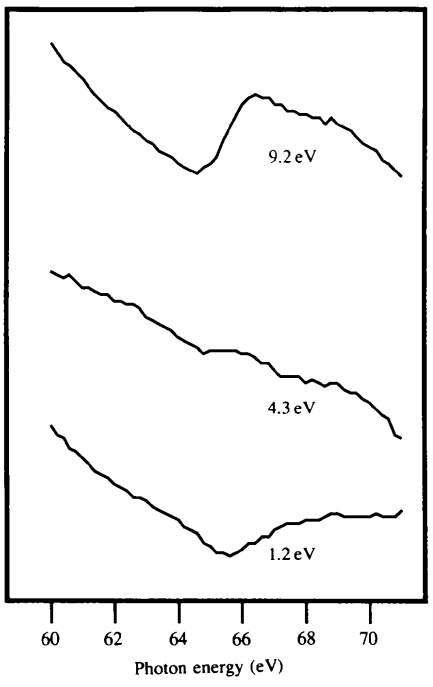

Figure 4
CIS spectra across the Ni $3p \rightarrow 3d$ threshold from scraped ceramic $La_2NiO_{4+\delta}$ at the valence-band edge (E_B = 1.2 eV), valence-band intensity maximum (E_B = 4.3 eV), and the satellite feature (E_B = 9.2 eV) showing anti-resonance at the valence-band edge, and resonance at the satellite. (The chosen initial-state binding energies are marked by arrows in Fig. 3.) Spectra are normalized to the beam monitor reading. The tungsten absorption coefficient of the beam monitor is featureless in this photon energy range.

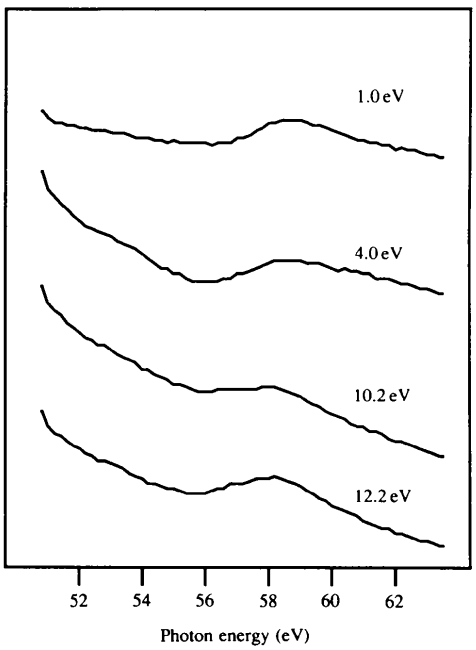

Figure 5
CIS spectra across the Fe $3p \rightarrow 3d$ threshold from scraped ceramic $La_{1.1}Sr_{0.9}Fe_{0.2}Ni_{0.8}O_{4+\delta}$ at the valence-band edge (E_B = 1.0 eV), valence band intensity maximum (E_B = 4.0 eV), and the satellite region (E_B = 10.2, 12.2 eV) showing resonance across the valence-band DOS. Spectra are normalized to the beam monitor reading. The tungsten absorption coefficient of the beam monitor is featureless in this photon energy range.

than in the central part of the valence band. Configuration interaction calculations for Fe_2O_3 show that the Fe contribution to the main part of the valence band arises mainly from a screened $d^5\underline{L}^1$ final state, with the satellite region arising from overlapping d^4 and $d^5\underline{L}^1$ contributions, peaking at around 13 eV binding energy (Fujimori *et al.*, 1986; Lad & Henrich, 1989). We would expect to see quite a strong resonance from the unscreened d^4 contribution, as sampled by our CIS data for 12.2 eV binding energy. Nevertheless, it is clear that there is a substantial contribution to the whole of the main valence band from Fe, with the O 2*p* states strongly hybridized with Fe throughout, as observed for simple Fe oxides (Fujimori *et al.*, 1986, 1987; Lad & Henrich, 1989). A similar broad valence-band contribution is observed for the neighbouring element, Co, in the complex oxide $Bi_2Sr_2CoO_{6+\delta}$ (Eisaki *et al.*, 1990). We note that, as in the simple oxides, the $d^5\underline{L}^1$ states appear to show resonant, rather than anti-resonant behaviour. However, the states sampled at 1 and 4 eV binding energies show a more pronounced dip prior to resonance than the satellite states, with a delayed resonance maximum at 58.6 eV compared with 58.2 eV for the satellite features, which we suggest is indicative of their screened nature.

Analogous satellite resonances are now well established at the Cu $3p \rightarrow 3d$ threshold in cuprate superconductors (*e.g.* List *et al.*, 1989; Shen *et al.*, 1989; Eisaki *et al.*, 1990; Flipse *et al.*, 1992), and are again attributed to the unscreened final state, in this case $3d^8$. Any anti-resonance in the states at the valence-band edge appears to be very weak compared with the corresponding nickelates or absent (*e.g.* List *et al.*, 1989; Shen *et al.*, 1989; Eisaki *et al.*, 1990, 1992). This difference has been attributed to the fact that in the cuprates this part of the DOS is mainly composed of $3d^9\underline{L}^1$ final states, which cannot be accessed *via* intra-atomic Auger decay of the type shown above (as this creates two holes in the *d* levels in the final state) (Eisaki *et al.*, 1992).

3.2.3. *$Bi_2Sr_2Ca_{1-x}Y_xCu_2O_{8+\delta}$* Here we have monitored the satellite resonance of $Bi_2Sr_2Ca_{1-x}Y_xCu_2O_{8+\delta}$ as a function of Y-doping level The formal Cu valency in this material moves from *ca* 2.3 for $x = 0$ to 2.0 for $x = 1$, with corresponding changes in the Cu–O hybridization in the copper/oxygen planes of the layer structure. Fig. 6 shows valence-band EDC's recorded with photon energies in the range 70–80 eV (encompassing the Cu $3p \rightarrow 3d$ resonance at ~74 eV photon energy) using station 6.2, for a superconducting sample with $x = 0$. This shows the main valence-band region, in the range 1–8 eV binding energy, a small DOS at E_F, and the satellite feature in the range 10–13 eV. The satellite resonance is evident most clearly as a small increase in intensity at 12.5 eV binding energy when the photon energy is increased from 74 to 74.5 eV. In square-planar coordination (D_{4h}) symmetry (corresponding to the CuO_2 planes in cuprate superconductors) the d^8 states giving rise to the satellite feature span singlet and triplet irreducible representations. The triplet states in the cuprate superconductors and in CuO are expected to resonate less strongly than the singlet states (Ghijsen *et al.*, 1990). This is mainly due to the presence of a ^1G final state with binding energy *ca* 12.5 eV, which has a significantly higher Auger decay matrix element than the singlet states at *ca* 10 eV binding energy (Eskes, Tjeng & Sawatzky, 1990). The net effect is that whilst the satellite feature spans the range 10–13 eV binding energy, the strongest resonant enhancement is expected at 12.5 eV, as observed here. Comparable EDC data have been collected for compositions between $x = 0$ and $x = 1$, and these are displayed in Fig. 7, essentially in the form of reconstructed CIS data. This is obtained by integrating the areas of the satellite peak and of the main valence band for each EDC. The ratio between the two is then plotted in Fig. 7 as a function of both doping level and photon energy. As the main valence band does not show any pronounced resonant behaviour, this procedure essentially leads to a description of the resonant behaviour of the satellite with photon energy. This reveals a structure in which two peaks are just discernible, and is in this respect very similar to the data of Shen *et al.* (1989) for the $x = 0$ composition, where a similar structure to the resonance is just perceptible. This structure is seen much more clearly in the resonant photoemission of CuO (Ghijsen *et al.*, 1990). The excited state created at resonance is $\{3p^5 3d^{10}\}^*$, with a full 3*d* shell. The shape of the resonance then reflects only the spin-orbit splitting of the 3*p* hole state into $3p_{3/2,1/2}$ multiplets, leading to the characteristic

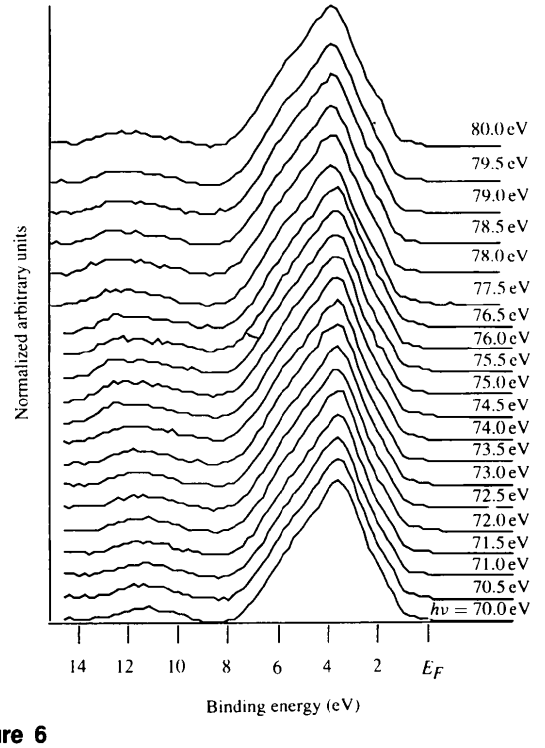

Figure 6
EDC's showing the valence-band and satellite region of a scraped ceramic sample of $Bi_2Sr_2Ca_{1-x}Y_xCu_2O_{8+\delta}$ ($x = 0$) across the Cu $3p \rightarrow 3d$ resonance at around 74 eV photon energy. Spectra are normalized to the beam monitor reading.

two-peaked structure (Thuler, Benbow & Hurych, 1982). In the case of CuO, this spin-orbit splitting is of the order of 2.1–2.2 eV (Ghijsen *et al.*, 1990; Thuler *et al.*, 1982), and appears invariant with Cu oxidation state (Thuler *et al.*, 1982). In our data, in the cases where the two-peaked structure is most evident, we measure a splitting of 2.2 eV (for the 75% Y-substituted sample, $x = 0.75$) and 2.1 eV (for the 50% Y-doped sample, $x = 0.5$), in good agreement with these literature values.

For the completely Y-substituted sample ($x = 1.0$), which is essentially a Cu^{II} material, the maximum of the resonance appears at 74.2 eV, in good agreement with the value of 73.8 eV estimated from the data of Ghijsen *et al.* (1990) for CuO. The resonance maximum shifts by around 0.8 eV to higher photon energy with decreasing Y content (increasing formal Cu valency). Thuler *et al.* (1982) have shown that the position of the Cu satellite resonance is affected by oxidation state, but that the shifts observed between Cu, Cu_2O (Cu^I) and CuO (Cu^{II}) are not linear with oxidation state. The observed shift is the resultant of shifts in the initial and final states of the 3*p* excitation.

Shifts in 3*p* core-level peaks in XPS on doping have not been measured for the complex oxide, as these features are very weak. However, shifts in the 2*p* core-level features, and in the valence-band edge with doping have been reported by a number of authors (*e.g.* van Veenendaal *et al.*, 1993, 1994; Itti *et al.*, 1991; Mante *et al.*, 1992; Golden *et al.*, 1991). There is general agreement that the valence-band edge moves towards the Fermi energy on hole doping, *i.e.* as the formal valency of Cu increases ($x \rightarrow 0$) (van Veenendaal *et al.*, 1993, 1994; Itti *et al.*, 1991; Mante *et al.*, 1992; Golden *et al.*, 1991). However, shifts in the 2*p* peak energies appear somewhat controversial. Comparison of literature spectra for Cu_2O (Cu^I), CuO (Cu^{II}) and $NaCuO_2$ (Cu^{III}) leads to the conclusion that the 2*p* binding energies increase with Cu valence (Golden *et al.*, 1991, and references therein). Consistent with this, these authors note a shift of the main Cu $2p_{3/2}$ feature of 0.4 eV to higher binding energy between 100% Y and 0% Y doping levels in $Bi_2Sr_2Ca_{1-x}Y_xCu_2O_{8+\delta}$, corresponding to an estimated Cu valence change from 1.9 to 2.3 (Golden *et al.*, 1991). A similar shift to high binding energy with increasing Cu valence is seen for $YBa_2Cu_3O_{7-\delta}$; here the formal copper valency is controlled by changing the oxygen content of the material (Gourieux *et al.*, 1988; Flavell & Egdell, 1989; Dauth, Kachel, Rupp & Gudat, 1988; Herzog, Schwarz, Sixl & Hoppe, 1988; Steiner *et al.*, 1987). However, a *decrease* in binding energy with increasing Cu valence is observed in $Bi_2Sr_2Ca_{1-x}Y_xCu_2O_{8+\delta}$ by van Veenendaal *et al.* and Itti *et al.* (although the latter authors use a bond-valence-sum calculation to arrive at the conclusion that the reverse behaviour is expected) (van Veenendaal *et al.*, 1993, 1994; Itti *et al.*, 1991). This discrepancy may arise in part from differences in procedures for charge referencing the spectra between different groups [as the samples with high Y contents (lower Cu valency) are not metallic]. The main feature of the Cu^{II} $2p_{3/2}$ multiplet corresponds to a $2p^5 3d^{10}\underline{L}^1$ final state having a similar full 3*d* level to the excited state created at the $3p \rightarrow 3d$ resonance, $\{3p^5 3d^{10}\}^*$. We might therefore expect both processes to be affected similarly by change in oxidation state. We suggest that the resonant behaviour of Fig. 7 supports the observation of an increase in binding energy with formal oxidation state for the Cu 2*p* levels in $Bi_2Sr_2Ca_{1-x}Y_xCu_2O_{8+\delta}$. These levels then move in the opposite direction to the valence-band edge on doping, suggesting that the doping behaviour is not explained by a simple doped semiconductor picture with a rigid shift of all core and valence levels (van Veenendaal *et al.*, 1993, 1994).

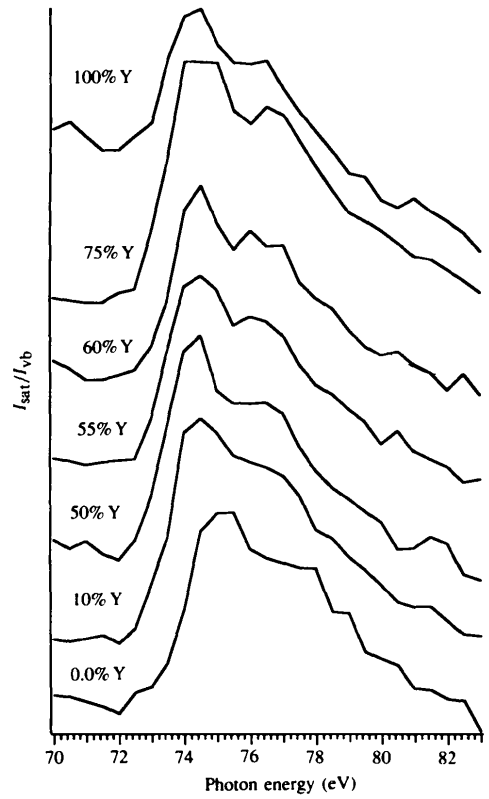

Figure 7
Reconstructed CIS spectra as a function of Y-doping level from EDC's of $Bi_2Sr_2Ca_{1-x}Y_xCu_2O_{8+\delta}$. The ratio of intensities of the satellite feature (I_{sat}) to the main valence band (I_{vb}) is plotted as a function of photon energy, through the Cu $3p \rightarrow 3d$ resonance at *ca* 74 eV. The spectra were normalized to the beam monitor reading prior to integration. The tungsten absorption coefficient of the beam monitor is featureless in this photon energy range.

4. Conclusions

Resonant photoemission in the VUV range is extremely powerful in determining the atomic character of the valence-band density of states in complex oxides. Subtle changes in formal oxidation state induced by counter-cation doping may be studied, and the information gained may in turn be used to infer the likely stability of cations in unusual valence states in these materials.

Specifically for the systems studied here we show that:

(*a*) For $Nd_2Ni_{1-x}Cu_xO_4$, like Nd_2CuO_4, the 4*f* contribution to the low-binding-energy-part valence-band DOS does not extend to the valence-band edge, suggesting that it may be possible to stabilize Ni^I and Cu^I in this structure on co-doping Ce for Nd.

(*b*) For $La_{2-x}Sr_xNi_{1-y}Fe_yO_{4+\delta}$ the resonant behaviour at the Fe $3p \rightarrow 3d$ threshold suggests that in this material, Fe is maintained in an oxidation state ≥ 3.0.

(*c*) Resonant behaviour at the Cu $3p \rightarrow 3d$ threshold may be used to monitor the modulation in Cu valency on doping Y into $Bi_2Sr_2Ca_{1-x}Y_xCu_2O_{8+\delta}$.

This work was funded by EPSRC and ICI Katalco.

References

Benloucif, R., Nguyen, N., Greneche, J. M. & Raveau, B. (1991). *J. Phys. Chem. Solids*, **52**, 381–387.

Dauth, M. B., Kachel, T., Rupp, B. & Gudat, W. (1988). *Physica C*, **153–155**, 153–154.

Eisaki, H., Takagi, H., Uchida, S., Matsubara, H., Suga, S., Nakamura, M., Yamaguchi, K., Misu, A., Namatame, H. & Fujimori, A. (1990). *Phys. Rev. B*, **41**, 7188–7191.

Eisaki, H., Uchida, S., Mizokawa, T., Namatame, H., Fujimori, A., van Elp, J., Kuiper, P., Sawatzky, G. A., Hosoya, S. & Katayama-Yoshida, H. (1992). *Phys. Rev. B*, **45**, 12513–12521.

Eskes, H., Tjeng, L. H. & Sawatzky, G. A. (1990). *Phys. Rev. B*, **41**, 288–299.

Flavell, W. R. & Egdell, R. G. (1989). *Phys. Rev. B*, **39**, 231–235.

Flipse, C. F. J., Lindsay, R., Raikar, G. N., Wincott, P. L., Thornton, G., Laverty, J. R. & Flavell, W. R. (1992). *Physica C*, **193**, 309–313.

Fujimori, A., Kimizuka, N., Taniguchi, M. & Suga, S. (1987). *Phys. Rev. B*, **36**, 6691–6693.

Fujimori, A., Saeki, M., Kimizuka, N., Taniguchi, M. & Suga, S. (1986). *Phys. Rev B*, **34**, 7318–7327.

Ghijsen, J., Tjeng, L. H., Eskes, H., Sawatzky, G. A. & Johnson, R. L. (1990). *Phys. Rev. B*, **42**, 2268–2274.

Golden, M. S., Golden, S. J., Egdell, R. G. & Flavell W. R. (1991). *J. Mater. Chem.* **1**, 63–68.

Gourieux, T., Krill, G., Maurer, M., Ravet, M. F., Menny, A., Tolentino, H. & Fontaine, A. (1988). *Phys. Rev. B*, **37**, 7516–7524.

Groen, W. A., de Leeuw, D. M. & Feiner, L. F. (1990). *Physica C*, **165**, 55–61.

Herzog, W., Schwarz, M., Sixl, H. & Hoppe, R. (1988). *Z. Phys. B*, **71**, 19–22.

Howlett, J. F., Flavell, W. R., Mian, M., Hollingworth, J., Hashim, Z., Aghabozorg, H. R., Squire, S., Wincott, P. L. & Downes, S. (1995). In preparation.

Itti, R., Munakata, F., Ikeda, K., Yamauchi, H., Koshizuka, N. & Tanaka, S. (1991). *Phys. Rev. B*, **43**, 6249–6252.

Lad, R. J. & Henrich, V. E. (1989). *Phys. Rev. B*, **39**, 13478–13485.

List, R. S., Arko, A. J., Bartlett, R. J., Olson, C. G., Yang, A.-B., Liu, R., Gu, C., Veal, B. W., Chang, Y., Jiang, P. Z., Vandervoort, K., Paulikas, A. P. & Campuzano, J. C. (1989). *Physica C*, **159**, 439–442.

Mante, G., Schmalz, Th., Manzke, R., Skibowski, M., Alexander, M. & Fink, J. (1992). *Surf. Sci.* **269–270**, 1071–1076.

Manthiram, A. & Goodenough, J. B. (1988). *Appl. Phys. Lett.* **53**, 420–422.

Massidda, S., Hamada, N., Yu, J. & Freeman, A. J. (1989). *Physica C*, **157**, 571–574.

Namatame, M., Fujimori, A., Tokura, Y., Nakamura, M., Yamaguchi, K., Misu, A., Matsubara, H., Suga, S., Eisaki, H., Ito, T., Takagi, H. & Uchida, S. (1990). *Phys. Rev. B*, **41**, 7205–7208.

Shen, Z.-X., Lindberg, P. A. P., Soukiassian, P., Eom, C. B., Lindau, I., Spicer, W. E. & Geballe, T. H. (1989). *Phys. Rev. B*, **39**, 823–826.

Steiner, P., Kinsinger, V., Sander, I., Siegwart, B., Hüfner, S., Politis, C., Hoppe, R. & Müller, H. P. (1987). *Z. Phys. B*, **67**, 497–502.

Tamegai, T., Koga, K., Suzuki, K., Ichihara, M., Sakai, F. & Iye, Y. (1989). *Jpn. J. Appl. Phys.* **28**, L112–115.

Thuler, M. R., Benbow, R. L. & Hurych, Z. (1982). *Phys. Rev. B*, **26**, 669–677.

Thuler, M. R., Benbow, R. L. & Hurych, Z. (1983). *Phys. Rev. B*, **27**, 2082–2088.

Tokura, Y., Takagi, H. & Uchida, S. (1989). *Nature (London)*, **337**, 345–347.

Veenendaal, M. A. van, Sawatzky, G. A. & Groen, W. A. (1994). *Phys. Rev. B*, **49**, 1407–1416.

Veenendaal, M. A. van, Schlatmann, R., Sawatzky, G. A. & Groen, W. A. (1993). *Phys. Rev. B*, **47**, 446–450.

Weller, M. T. (1992). Personal communication.